Nonstoichiometric Properties of Nanoporous Iron Oxide Films

N. Uekawa*

Department of Applied Chemistry, Faculty of Engineering, Chiba University, 1-33 Yayoi-cho, Inage-ku, Chiba-shi 263, Japan

K. Kaneko

Department of Chemistry, Faculty of Science, Chiba University, 1-33 Yayoi-cho, Inage-ku, Chiba-shi 263, Japan

Received: May 15, 1998; In Final Form: September 1, 1998

Porous iron oxide films were prepared by the polymer precursor method with poly(vinyl alcohol) (PVA). Pore size distribution of the films was determined by the N_2 adsorption isotherm at 77K with the aid of the quartz crystal microbalance method. The crystal and pore structures of the iron oxide film varied with the amount of PVA in a coating solution; the crystal structure changed from α-Fe_2O_3 to γ-Fe_2O_3 with an increase of PVA. XPS valence band spectra showed the presence of the layer of Fe_3O_4 in a mixed valence state on the surface of the microporous film. Also the temperature dependence of the electrical resistance of the film showed the presence of the Fe_3O_4 like layer on the film surface. The kinetics of the reduction of the porous iron oxide films was examined, and the activation energy of the reduction was determined. The Gibbs free energy of the film reduction of α-Fe_2O_3 to Fe_3O_4 decreased. Hence, it was shown that the surface energy of the porous films controls the crystal and surface structures of the film.

Introduction

Solid surfaces and interfaces have different properties from the bulk solid. Atoms on the surface have special structures such as reconstruction or relaxation, and the energy of the solid surface is greater than that of the bulk solid. The whole excess energy of the atoms on the surface is defined as surface energy.[1]

To reduce the surface energy, gas molecules or impurities in the bulk are adsorbed or segregated at the surface. Hence, porous solids with a high surface area have excellent adsorptive properties, which have been widely applied in various technologies.[2−4] There are a variety of attempts to develop a new porous solid such as a regular mesoporous silica (MCM-41) by the templating method.[5,6] However, it is expected that the great surface energy induces not only a marked adsorption but also a specific surface structure. Larkins et al. showed that the formation energy of Ni metal from the NiO fine powder of the surface area = ca. 100m^2/g is smaller than that from bulk NiO by the surface energy.[7] The ratio of surface atoms to whole atoms of a porous film is larger than that of the powder;[8−11] the porous film is a good system to examine the effect of the surface energy on the surface structure.[12,13]

Representative iron oxides are α-Fe_2O_3, γ-Fe_2O_3, and Fe_3O_4. γ-Fe_2O_3 and Fe_3O_4 have the spinel structure, while α-Fe_2O_3 has the corundum structure. Further, iron oxides show n-type semiconductivity.[14] γ-Fe_2O_3 and Fe_3O_4 are metastable in the oxidative atmosphere so that the spinel iron oxide is oxidized to α-Fe_2O_3 by heating above 673 K. Thereby, the porous iron oxide films are appropriate systems to investigate how the surface energy of the porous film influences their surface structures through the crystal structure transformation.[15]

In this study, the thin film of porous iron oxide was prepared by the polymer precursor method.[16−18] The high microporosity of the film was directly determined by the N_2 adsorption isotherm with the aid of the quartz crystal microbalance (QCM) method.[19,20] The explicit atmosphere-sensitive nature of the microporous iron oxide film was discussed with the relevance to the surface energy.

Experimental Section

Preparation of Porous Iron Oxide Films. The porous iron oxide films were prepared by the polymer precursor method (PP method) with poly(vinyl alcohol) (PVA). This preparation method is tentatively named "PVA-PP method". Iron(III) nitrate enneahydrate ($Fe(NO_3)_3 \cdot 9H_2O$) (0.005 mol), citric acid monohydrate (0.02 mol), ethylene glycol (0.05 mol), and PVA (0.55 g) (n = 500, PVA/(citric acid monohydrate) = 0.13 weight ratio) were dissolved in 100 mL of distilled water. This solution was heated until the evolution of NO_x was observed. The resulting viscous solution contains the polymer complex among iron(III) ions, PVA, and the polyether formed from citric acid and ethylene glycol. The polymer complex was dissolved in 25 mL of methanol to make the coating solution. Films were prepared by the spin-coating technique at 2000 rpm for 10 s on the Pyrex glass substrate (50 mm × 25 mm × 2 mm) with 1 mL of the coating solution. The film was calcined at 773 K for 5 min in air. To get an uniform film, the coating followed by the calcination was repeated 20 times. Hereinafter, the iron oxide film prepared by the above procedure is tentatively named "Fe-0.13". Here, the figure of 0.13 is the weight ratio of PVA/(citric acid monohydrate). Other films were prepared using different PVA/(citric acid monohydrate) weight ratios of 0, 0.13, 0.26, 0.52, 0.79, 1.05, and 1.31 in order to control the pore size distribution.

N_2 Adsorption Measurement by the QCM Method. The N_2 adsorption isotherm of the iron oxide film was measured at 77 K by the QCM method. The amount of the adsorbed N_2

10.1021/jp982249x CCC: $15.00
Published on Web 10/14/1998

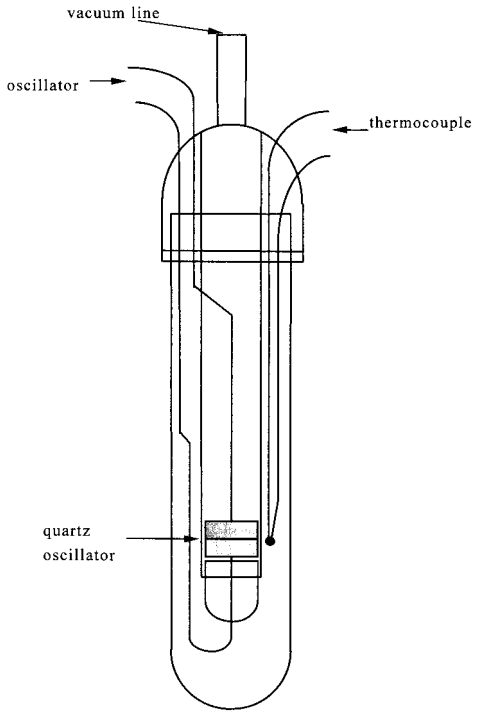

Figure 1. Schematic representation of the vacuum glass cell for measuring N_2 adsorption isotherm by the quartz oscillator microbalance method.

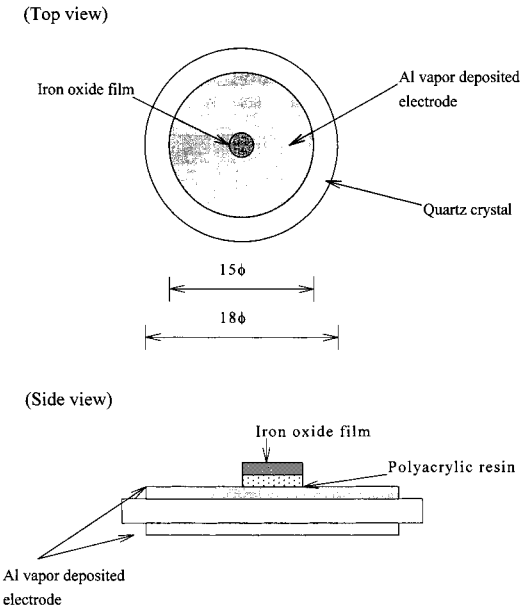

Figure 2. Schematic representation of the quartz crystal with the iron oxide film.

was detected with an ultimate sensitivity of 10^{-8} g. Figure 1 illustrates the schematic representation of the cell for the adsorption measurement. The AT-cut quartz crystal of characteristic vibration frequency equal to 6 MHz was used. The shape of Al electrodes on the quartz crystal is illustrated in Figure 2. The iron oxide film was stuck on the Al electrode with a polyacrylic resin.

The adsorption measurement was carried out as follows: The oscillating frequency (f_1) of the crystal with the polyacrylic resin was measured at room temperature. The iron oxide film was stuck on the crystal, and the oscillating frequency (f_2) was measured at room temperature (298 K) after the pretreatment at 383 K in 1 mPa for 2 h. After the cell was cooled at 77 K, the frequency (f_3) was measured before N_2 adsorption. The frequency (f_4) was measured during N_2 adsorption at 77 K. The weight of adsorbed species on the quartz crystal is proportional to the change of the oscillating frequency. The film weight and the amount of N_2 adsorbed are $k_1(f_2 - f_1)$ and $k_2(f_4 - f_3)$, respectively. Here, k_1 and k_2 are the proportional constant at 298 and 77 K, respectively. Thereby, the amount of the adsorbed N_2 per unit weight of the film is calculated as follows:[20]

$$\Delta W = k\frac{f_4 - f_3}{f_2 - f_1} \tag{1}$$

Here, ΔW is the amount of adsorbed N_2 on the film per unit weight of the film and k is the constant defined as k_2/k_1. To calculate the relative pore size distribution, the relation between the relative pressure and the amount of adsorbed N_2 is required and the absolute amount is not necessary. The value of k does not affect the relative pore size distribution. As it was difficult to measure k_2, which determines the k, the frequency shift of $(f_4 - f_3)/(f_2 - f_1)$ was used to calculate the relative pore size distribution.

Characterization. The crystal structure of the iron oxide film was examined by X-ray diffraction (XRD) using Cu Kα radiation (45 kV, 20 mA) with a Ni filter. The morphology of the film was observed by a scanning electron microscope (SEM). The thickness of the film was measured by the optical multiple reflection interference method, and the thickness was ca. 50 nm per coating. The films used for measuring the electrical resistance and the N_2 adsorption were prepared by repeating the coating procedure 20 times, and the thickness was ca. 1 μm. The electrical resistance of the iron thin oxide film on the Pyrex glass substrate was measured in vacuo after the pretreatment at 393 K and 1 mPa for 2 h. The Al electrode was formed on the films by a vacuum evaporation coating. The $I-V$ characteristics of the films supported the ohmic contact between the iron oxide film and the Al electrode. The electrical resistance was measured from the current under a constant voltage with a surface conductive type cell with a square area of 12 × 12 mm^2 using an electronic picoammeter (Keithley 485). An Shimazu ESCA 850 was used for recording XPS spectra. The base pressure was $<10^{-6}$ Pa, and Mg Kα radiation (7kV 30mA) was used. The binding energy was referred to the C(1s) binding energy of 285.0 eV.

Results and Discussion

The Pore Size Distribution of the Iron Oxide Film. Figure 3 shows the N_2 adsorption isotherms of the iron oxide films prepared by the PVA-PP method. The amount of adsorbed N_2 increases with the increase of the PVA/(citric acid monohydrate) ratio. Hence, the pore volume of the film becomes greater with the increase of PVA. The steep increase of the amount adsorbed is observed below $P/P_0 = 0.1$, indicating the presence of micropores. The increase of N_2 adsorption above $P/P_0 = 0.8$ stems from adsorption on the external surface and mesopores.

Figure 4 shows pore size distributions calculated by the Cranston−Inkley method.[21] The Kelvin equation cannot be applied to absorption on micropores, and we must be cautious of the pore size distribution in the micropore range calculated by the Cranston−Inkley method. However, the qualitative interpretation in the micropore region is possible. Figure 4a shows the pore size distribution of Fe-0.13, which indicates that the film has mesopores in the range of 2.0−3.5 nm. Micropores develop in Fe-0.26 and Fe-0.79 compared with mesopores, as shown in Figure 4b,c. Thus, the iron oxide film prepared by

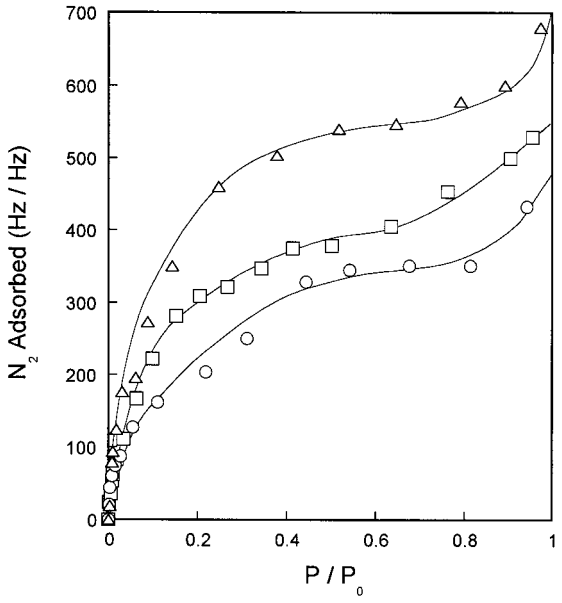

Figure 3. N_2 adsorption isotherms of the iron oxide films prepared by the PVA-PP method at 77 K: ○, Fe-0.13; □, Fe-0.26; △, Fe-0.79.

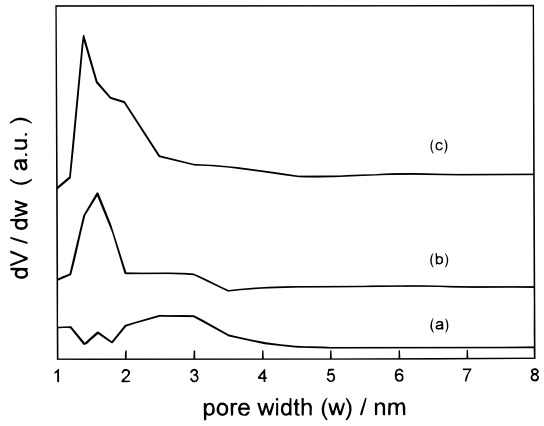

Figure 4. Pore size distribution of the iron oxide films prepared by the PVA-PP method with Cranston−Inkley analysis: (a) Fe-0.13, (b) Fe-0.26, and (c) Fe-0.79.

the PVA-PP method becomes microporous with an increase of the amount of PVA in the polymer precursor. This is because evolution of gases due to the thermal decomposition of PVA produces micropores. We can control the pore structure of the iron oxide film by addition of PVA. Also the considerably great external and mesopore surface areas suggest that these films are composed of fine particles having micropores.

Morphology and Structure of Iron Oxide Films. Figure 5 shows the scanning electron microscopic (SEM) images of Fe-0.52, which was prepared by repeating the coating procedure 20 times. Thickness of the film was uniform, as shown in Figure 5a. Figure 5b shows that the film consists of the ellipsoidal particles whose diameter is ca. 100 nm. The micropores should be in the ellipsoidal particles, while the mesopores should come from the interparticle voids. Figure 6 shows the X-ray diffraction patterns of iron oxide films. All diffraction peaks of Fe-0, Fe-0.52, and Fe-0.79 were assigned to α-Fe_2O_3. However, X-ray diffraction patterns of Fe-1.05 and Fe-1.31 are different from that of pure α-Fe_2O_3. The XRD pattern of Fe-1.05 has the additional weak patterns stemming from α-Fe_2O_3. Fe-1.05 is the mixture of α-Fe_2O_3 and γ-Fe_2O_3. Fe-1.31 is pure γ-Fe_2O_3. It is well-known that γ-Fe_2O_3

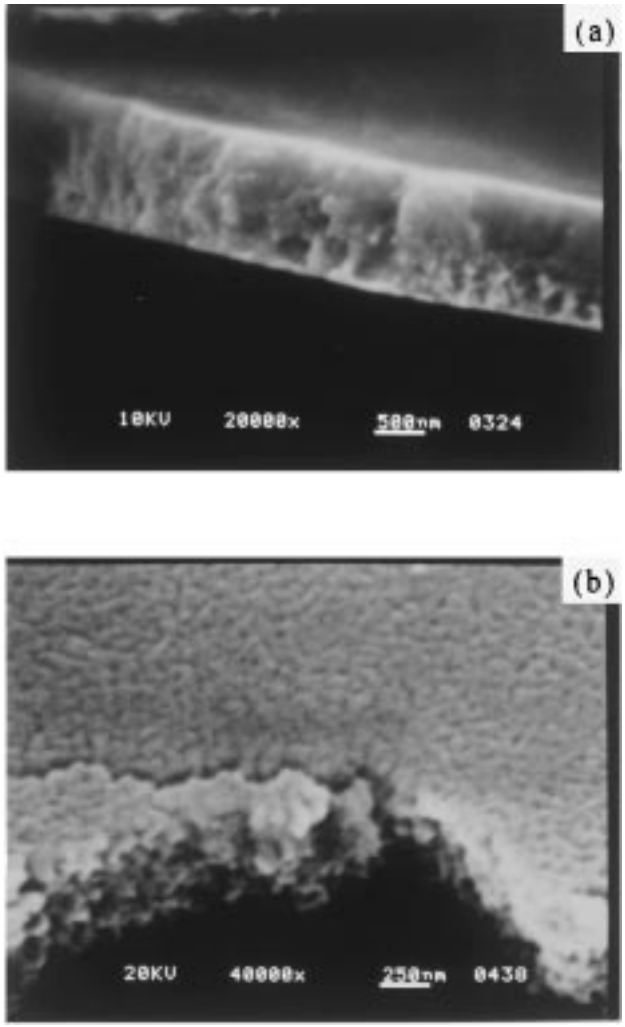

Figure 5. Scanning electron microscopic images of the iron oxide film (Fe-0.52) prepared by the PVA-PP method: (a) sectional view and (b) top view.

transforms into α-Fe_2O_3 by heating above 673 K. Hence γ-Fe_2O_3 is a metastable structure at 773 K that is the calcination temperature of the precursor of the films. However, γ-Fe_2O_3 is stable in these microporous iron oxide films of Fe-1.05 and Fe-1.31. It is noteworthy that the metastable γ-Fe_2O_3 structure is stabilized in the microporous film.

The Reduced Surface Structure of Porous Iron Oxide Film. Figure 7 shows XPS valence band spectra of the prepared iron oxide films and pure powdered Fe_3O_4. Although the valence band peaks are very broad, a careful analysis provides the characteristic feature from one sample to another. The peaks around 5.0 eV of Fe-0 (see Figure 7a) are assigned to the band due to localized 3d electrons. This band has three peaks due to 3d orbitals split by the O^{2-} octahedrally coordinated field. The peaks can be assigned to the 3d energy levels of ^3e_g, $^2t_{2g}$, and ^2e_g, as described in Figure 7. This spectrum is the same as that of powdered α-Fe_2O_3.[22]

The peak intensities of ^3e_g around 2.0 eV and ^2e_g around 8.0 eV become smaller with an increase of the PVA content. That is, the peak intensities of the oxide film are reduced with the increase of the microporosity. The XPS valence band spectra of Fe-0.52, Fe-1.05, and Fe-1.31 are similar to those of pure Fe_3O_4. The XRD data of these films showed that the structures are not Fe_3O_4 but α-Fe_2O_3 or γ-Fe_2O_3, as shown before. Accordingly, just the thin layer of these oxide films should be

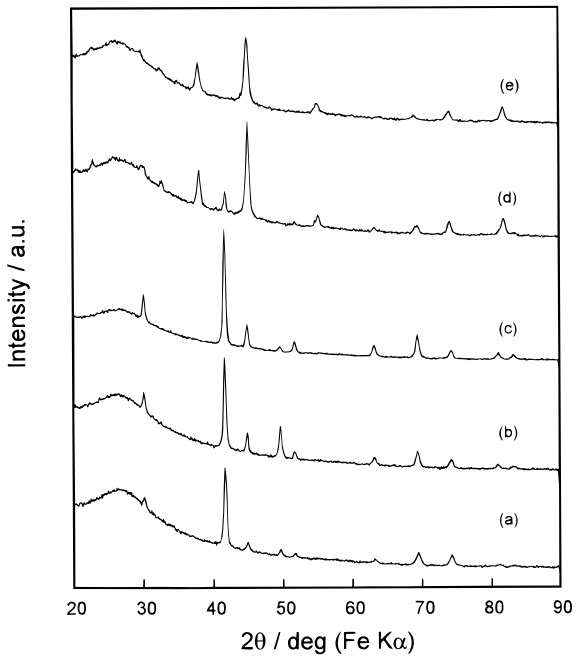

Figure 6. X-ray diffraction patterns of the iron oxide films prepared by the PVA-PP method: (a) Fe-0, (b) Fe-0.52, (c) Fe-0.79, (d) Fe-1.05, and (e) Fe-1.31.

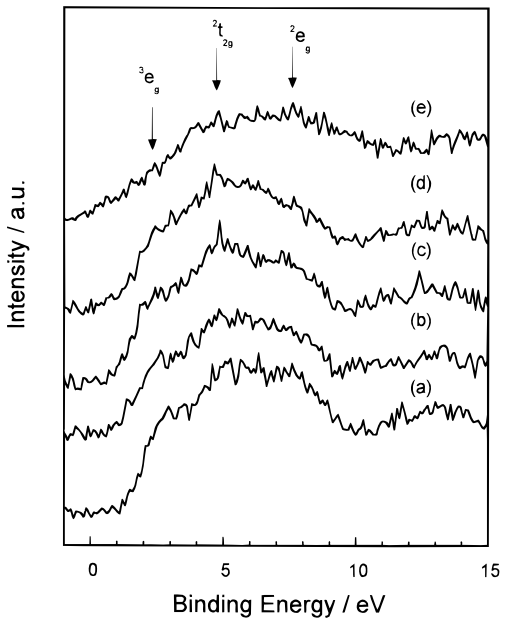

Figure 7. XPS valence band spectra of the iron oxide films prepared by the PVA-PP method: (a) Fe-0, (b) Fe-0.52, (c) Fe-1.05, (d) Fe-1.31, and (e) Fe_3O_4 films.

the Fe_3O_4 structure with the mixed valence state. The high surface energy contributes to the stabilization of the Fe_3O_4 layer on the film surface.

The Fe_3O_4 thin layer on the microporous film was also investigated by measuring the change in the temperature dependence of the electrical resistance R of the films (Figure 8). The logarithm of electrical resistance R vs T^{-1} relation is divided into two linear plots at 435 K except for Fe-0. The slope of the linear relation above 435 K is greater than that below 435 K. The activation energies for electronic conduction were determined from the slopes. Here, the activation energies below and above 435 K will be designated $E_a(1)$ and $E_a(2)$.

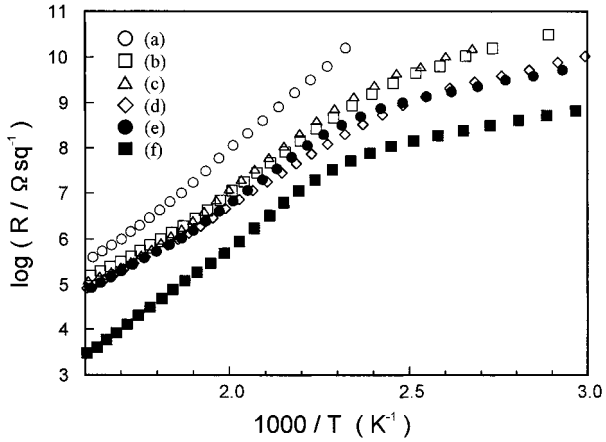

Figure 8. Temperature dependences of the electrical resistance of the iron oxide films prepared by the PVA-PP method: (a) Fe-0, (b) Fe-0.26, (c) Fe-0.52, (d) Fe-0.79, (e) Fe-1.05, and (e) Fe-1.31.

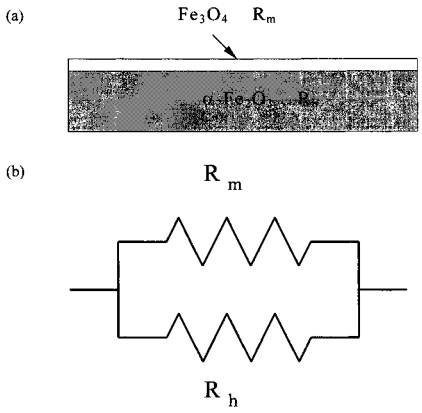

Figure 9. Schematic representation of the iron oxide films: (a) the iron oxide film in the reduction process and (b) the equivalent circuit.

The obtained $E_a(1)$ values are in the range of 0.26−0.36 eV. According to the literature,[23−26] the activation energies of Fe_3O_4 and Fe_2O_3 are in the range of 0.1−0.2 eV and in the range of 1.0−2.2 eV, respectively. $E_a(1)$ is close to the activation energy of Fe_3O_4, supporting the presence of the Fe_3O_4 thin layer on the surface of the microporous iron oxide films. On the other hand, $E_a(2)$ values were in the range of 0.97−1.02 eV. $E_a(2)$ is close to the activation energy of electronic conduction for α-Fe_2O_3. Thus, the electrical resistance data agree with the XPS results.

Mechanism of Surface Reduction of Oxide Films. In the above, it was shown that only the surface of α-Fe_2O_3 is reduced with the increase of the microporosity. The reduction can be described by eq 2.

$$^3/_2Fe_2O_3 \rightarrow Fe_3O_4 + {}^1/_4O_2 \qquad (2)$$

The electrical conductivity measurement of the surface layer of the iron oxide film at a constant temperature gives the information on the film reduction by the following reason. The structure of the oxide film can be described by the two-layer model, as illustlated in Figure 9a. That is, only the superficial layer of the oxide film is Fe_3O_4, and the bulk structure of the film is α-Fe_2O_3. Accordingly, the resistance of the film, R, can be described by the parallel-type electrical equivalent circuit of two resistances R_m and R_h, as illustrated in Figure 9b. R_m and R_h denote the resistances of the magnetite and α-Fe_2O_3

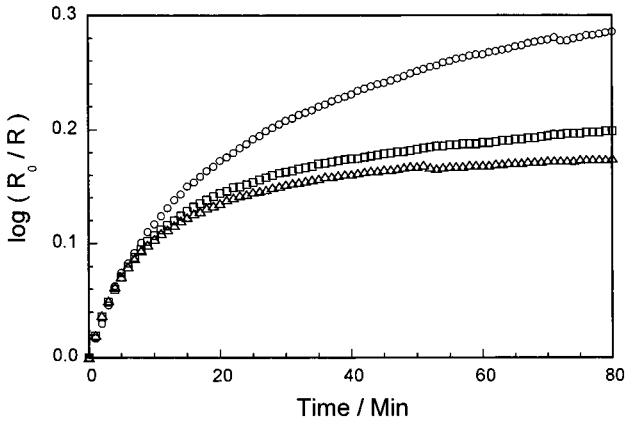

Figure 10. Electrical resistance change of the iron oxide film Fe-0 at different temperatures in 1 mPa: ○, 523 K; □, 548 K; △, 573 K.

(hematite) layers. As $R_m \ll R_h$, R is almost equal to R_m. R can provide the information on the content and crystallinity of the Fe_3O_4 layer. The total electrical resistance of the film is expressed by eq 3.

$$R = K/\sigma \tag{3}$$

where K is a constant that depends on the shape of the film. σ is the electrical conductivity of the Fe_3O_4 layer. σ is given by

$$\sigma = ne\mu \tag{4}$$

where e is the electrical charge of a carrier, n is the carrier concentration, and μ is the charge mobility. If the Fe_3O_4 layer has the same crystallinity regardless of different thicknesses and thereby μ is a constant, the electrical resistance is inversely proportional to the amount of the charge carrier. The change of the reciprocal of R with time gives the formation rate of the Fe_3O_4 layer because n is proportional to the Fe_3O_4 amount. Accordingly, the rate of the reduction of the film should be described by the R^{-1} vs t plot.

Figure 10 shows the time dependence of the electrical resistance of Fe-0 film at a constant temperature in 1 mPa; the electrical resistance decreases with the time markedly. The rate process of the structure transformation from α-Fe_2O_3 to Fe_3O_4 is considered to follow the first-order rate law. Hence, the time dependence also follows the first-order rate law, as described in eq 5.

$$\sigma = \sigma_\infty + (\sigma_0 - \sigma_\infty)\exp(-kt) \tag{5}$$

where σ_0 and σ_∞ are the electrical conductivity of the film at $t = 0$ and $t = \infty$, respectively. k is the first-order rate constant. Substituting σ in eq 5 for eq 3, we obtain eq 6.

$$R_0/R = C_{eq} + (1 - C_{eq})\exp(-kt) \tag{6}$$

where R_0 is the electrical resistance of the film at $t = 0$. k is the first-order rate constant, and C_{eq} is R_0/R at $t \rightarrow \infty$. This means that the rate-determining step of the reduction is the structure transformation from α-Fe_2O_3 to Fe_3O_4. The $\log(R_0/R)$ vs t curve was fitted to eq 6 by the nonlinear least-squares method (Gauss−Newton method). Figure 11 shows the Arrhenius plots of k. The plots follow the linear relation in the range of 500−600 K, and the activation energy E_a for the surface reduction was obtained from the slope of the plots. The E_a values of Fe-0, Fe-0.13, and Fe-0.26 were 50, 44, and 47 kJ/mol, respectively. From Figure 11, it is shown that the rate constant k tends to increase with the pore development. The

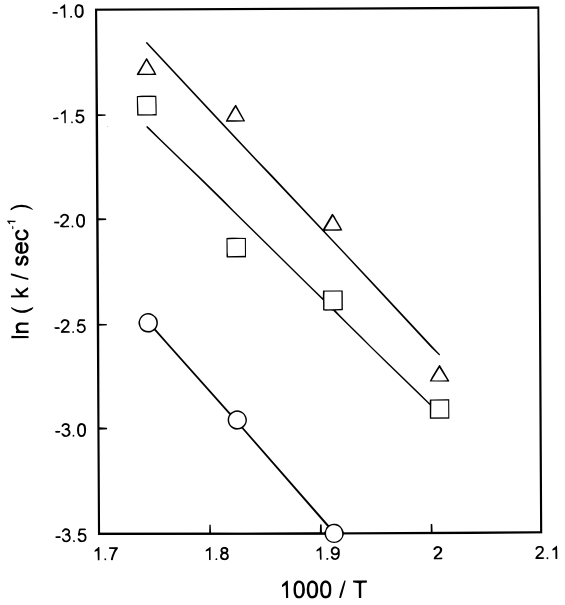

Figure 11. Arrhenius plot of the first-order rate constant k of the reduction of the iron oxide films: ○, Fe-0; □, Fe-0.13; △, Fe-0.26.

oxygen ions on the film surface are coordinately unsaturated. The coordinately unsaturated oxygen ions are easily eliminated from the surface. Hence, the specific surface area of the films increases with an increase of the microporosity, leading to the increase of the rate constant k.

The effect of the high surface area due to the microporosity on the Gibbs free energy of the reaction eq 2 is discussed here. The ΔG of the reaction eq 2 of the bulk phase is described as follows

$$\Delta G = \mu_{Fe_3O_4} + {}^1/_4\mu_{O_2} - {}^3/_2\mu_{\alpha-Fe_2O_3} \tag{7}$$

where, $\mu_{Fe_3O_4}$, μ_{O_2}, and $\mu_{\alpha-Fe_2O_3}$ are chemical potentials of Fe_3O_4, O_2, and α-Fe_2O_3, respectively. According to the Ellingham diagram, ΔG is in the range of 150−170 kJ/mol in the temperature range of 500−600 K.[15] Here, the activation energy of the reaction eq 2 of the thin film (E_a) was in the range of 44 and 50 kJ/mol. Thereby, the relation of $E_a < \Delta G$ holds. E_a is generally greater than ΔG_{film}, which is the Gibbs free energy of the reaction eq 2 of the thin films so that $\Delta G > E_a > \Delta G_{film}$ holds. Thereby, we conclude $\Delta G > \Delta G_{film}$. The reason for $\Delta G > \Delta G_{film}$ is considered as follows. ΔG_{film} is described by eq 8.

$$\Delta G_{film} = \mu_{Fe_3O_4} + {}^1/_4\mu_{O_2} - {}^3/_2\mu_{\alpha-Fe_2O_3} + S(\gamma_{Fe_3O_4} - {}^3/_2\gamma_{\alpha-Fe_2O_3}) \tag{8}$$

where $\gamma_{Fe_3O_4}$ and $\gamma_{\alpha-Fe_2O_3}$ are the surface excess free energies (surface tensions) of Fe_3O_4 and α-Fe_2O_3, respectively, and S is the specific surface area of the film per 1 mol of α-Fe_2O_3. $\gamma_{Fe_3O_4}$, $\gamma_{\alpha-Fe_2O_3}$, and S govern ΔG_{film}, as shown in eq 8. In particular, the relative value of $\gamma_{Fe_3O_4}$ and $\gamma_{\alpha-Fe_2O_3}$ determines the sign of $(\Delta G - \Delta G_{film})$. Fe_3O_4 and α-Fe_2O_3 have the crystal structure with filling cations in the octahedral and/or the tetrahedral site in a close-packed array of oxygen anions and some vacancies in cation sites. α-Fe_2O_3 has more cation vacancies than Fe_3O_4 so that the α-Fe_2O_3 surface has more coordinately unsaturated ions than the Fe_3O_4 surface. Thereby, it is considered that the surface excess free energy of α-Fe_2O_3 is larger than that of Fe_3O_4, that is, $\gamma_{Fe_3O_4} < \gamma_{\alpha-Fe_2O_3}$. Consequently $\Delta G > \Delta G_{film}$

is obtained. Therefore, the equilibrium given by eq 2 shifts to the formation of Fe_3O_4 on the iron oxide film surface, as shown in the experimental results.

Acknowledgment. The financial support by the Science Research Grant from the Ministry of Education, Japanese Government, is greatly appreciated.

References and Notes

(1) Zangwill, A. In *Physics at Surfaces*; Cambridge University Press: Cambridge, 1988; Chapter 1.
(2) Kaneko, K. In *Adsorption on New and Modified Inorganic Chemistry*; Dabrowski, A., Tertykh, V. A., Eds.; Elsevier: Amsterdam, 1996; p 573.
(3) Gregg, S. J.; Sing, K. S. W. *Adsorption, Surface Area and Porosity*, 2nd ed.; Academic Press: London, 1982; Chapter 4.
(4) Wang, Z. M.; Suzuki, T.; Uekawa, N.; Asakura, K.; Kaneko, K. *J. Phys. Chem.* **1992**, *96*, 10917.
(5) Kresge, C. T.; Leonowicz, M. E.; Roth, W. J.; Vartuli, J. C.; Beck, J. S. *Nature* **1992**, *359*, 710.
(6) Davis, M. E.; Burkett, S. L. *Zeolite* **1995**, *12*, 33.
(7) Larkins, F. P.; Fensham, P. J. *Nature (London)* **1967**, *215*, 1268.
(8) Uekawa, N.; Watanabe, M.; Kaneko, K. *J. Chem. Soc., Faraday Trans.* **1995**, *91*, 2161.
(9) Uekawa, N.; Kaneko, K. *J. Phys. Chem*. **1996**, *100*, 4193.
(10) Hench, L. L.; West, J. K. *Chem. Rev.* **1990**, *90*, 33.
(11) Zusman, R.; Rottman, C.; Ottolenghi, M.; Avnir, D. *J. Non-Cryst. Solids* **1990**, *122*, 107.
(12) Swalin, R. A. *Thermodynamics of Solids*; John Wiley & Sons: New York, 1962; Chapter 12.
(13) Pitzer, K. S. *Thermodynamics*; McGraw-Hill: New York, 1995; Chapter 23.
(14) Cox, P. A. *Transition Metal Oxides*; Clarendon Press: Oxford, 1995; p 134.
(15) Cochran, S. J.; Larkins, F. P. *J. Chem. Soc., Faraday Trans. 1* **1985**, *81*, 2179.
(16) Baythoun, M. S. G.; Sale, F. R. *J. Mater. Sci*. **1982**, *17*, 2757.
(17) Kakihana, M.; Yoshimura, M.; Mazaki, H.; Yasuoka, H.; Brjesson, L. *J. Appl. Phys*. **1992**, *71*, 3904.
(18) Tai, L.-W.; Lessing, P. A. *J. Mater. Res*. **1992**, *7*, 511.
(19) Thomas, J. H.; Sharma, S. P. *J. Vac. Sci. Technol*. **1976**, *13*, 549.
(20) Tsionski, V.; Gileadi, E. *Langmuir* **1994**, *10*, 2830.
(21) Cranston, R. W.; Inkley, F. A. *Adv. Catal.* **1957**, *9*, 143.
(22) Tossell, J. A.; Vaughan, D. J.; Johnson, K. H. *Nature* **1973**, *244*, 42.
(23) Kofstad, P. *Nonstoichiometry, Diffusion, and Electrical Conductivity in Binary Metal Oxides*; John Wiley & Sons: New York, 1962; p 232−236.
(24) Merchant, P.; Collins, R.; Kershaw, R.; Dwight, K.; Wold, A. *J. Solid State Chem*. **1979**, *27*, 307.
(25) Buchenau, U.; Muller, I. *Solid State Commun.* **1972**, *11*, 1291.
(26) Hardee, K. L.; Bard, A. J. *J. Electrochem. Soc*. **1977**, *124*, 215.